

High-Power Ultralow Divergence Edge-Emitting Diode Laser With Circular Beam

Lijie Wang, Cunzhu Tong, *Member, IEEE*, Sicong Tian, Shili Shu, Yugang Zeng, Jiamin Rong, Hao Wu, Enbo Xing, Yongqiang Ning, and Lijun Wang

Abstract—A recognized drawback of edge-emitting diode lasers is their high divergence and elliptical beam shape since the first diode laser was demonstrated. In this paper, we demonstrated the ultranarrow circular beam emission from the broad area diode laser based on a modified Bragg-like waveguide. The low vertical divergence of 9.8° with 95% power content and 4.91° with the full-width at half-maximum was realized in the devices with $150\ \mu\text{m}$ stripe width. The maximum output power was 4.2 W under quasi-continuous-wave operation and presently limited by thermal rollover. The detailed design principle was presented and it was found that reducing the refractive index and thickness of the defect layer was able to improve the vertical divergence and achieve the stable circular beam emission by controlling the lateral current distribution using the deep stripe. The packaged device with $90\ \mu\text{m}$ stripe width demonstrated a maximum continuous wave power of 4.6 W at $10\ ^\circ\text{C}$. A direct fiber coupling efficiency of 90.6% had been achieved with a common fiber of $105\ \mu\text{m}$ core diameter.

Index Terms—Semiconductor lasers, photonic bandgap, low-beam divergence, high-power diode lasers.

I. INTRODUCTION

HIGH power diode lasers are widely used for pumping of solid state lasers and fiber lasers, material processing, security and defense, typically coupled into a fiber for easy use by beam shaping and combining techniques. However, the conventional diode lasers usually suffer from a large vertical far-field (FF) divergence of more than 30° for the definition of full-width at half-maximum (FWHM) [1] and strongly elliptical beam because of the vertical optical confinement using narrow total interface reflection (TIR) waveguide, which is recognized as one of the main drawbacks [2] since the first edge-emitting diode laser was demonstrated in 1962. This drawback requires the use of expensive optical elements with high numerical aperture (NA) for focusing and coupling of diode lasers. Furthermore, the serious asymmetry of the vertical ($\sim 40^\circ$) and lateral ($\sim 10^\circ$) FF divergence angle also needs sophisticated circularly re-shaped optics for efficient coupling. Therefore, diode lasers with low

divergence and circular beam emission would be valuable for the direct applications.

Many approaches have been proposed to improve the vertical beam divergence of edge-emitting diode laser, including the super large optical cavity (SLOC) [3], asymmetric waveguide [4], [5], double barrier separate confinement heterostructures [6], multi-active region [7], and inserting anti-guiding layers [8]–[10]. These methods have reduced the vertical beam divergence with the definition of FWHM, $\theta_{\perp,\text{FWHM}}$, down to below 10° [10], however, the FF emission angle with 95% power content, $\theta_{\perp,95\%}$, is still high, which is more meaningful for the description of FF angle in the practical applications and must be minimized to eliminate unwanted stray light effects in the application such as pumping of the fiber cladding [11]. A low index quantum barrier structure combined with SLOC was proposed to improve the optical mode confinement and had demonstrated the $\theta_{\perp,\text{FWHM}}$ of 8° [11], [12]. The corresponding $\theta_{\perp,95\%}$ is as low as 15.6° , which was almost the best result reported for the edge-emitting diode lasers with watt-level power output. However, the further improvement of the divergence angle for this index-guiding laser is limited by the onset of high order transverse modes, and the realization of circular beam emission is also difficult.

In order to solve these problems, edge-emitting diode lasers based on the one-dimensional photonic crystal structure have been proposed, in which light is guided by the photonic bandgap (PBG) effect instead of TIR in the vertical direction [13]–[15]. As the PBG modes possess strong mode discrimination due to the large mode spacing and significant losses of high-order modes, the laser could achieve stable single mode lasing with large optical mode size [14]. Recently, a longitudinal photonic bandgap crystal (LPBC) laser has demonstrated the low $\theta_{\perp,\text{FWHM}} < 5^\circ$ [15]–[19], but the $\theta_{\perp,95\%}$ is still wide due to the existence of side lobes [20], which is about 20° estimated from the results in [18]. The relatively high $\theta_{\perp,95\%}$ is mainly caused by the deviation of beam profile from the ideal Gaussian shape. The LPBC lasers consist of an optical defect sandwiched between one periodic waveguide and one TIR waveguide. The refractive index of materials in the optical defect usually has a same or higher value than that of the highest index in the PBG waveguide [16]. The inherent optical waveguiding of the optical defect itself confines the optical mode tightly, resulting in a much higher near field (NF) intensity as in a Gaussian distribution. This will lead to a wide distribution of FF and limit the minimum achievable $\theta_{\perp,95\%}$ [12]. In contrast, a Bragg reflection waveguide (BRW) laser was proposed [21], [22], which utilized transverse Bragg reflectors on both sides and a low-index defect to expand the mode over the whole waveguide.

Manuscript received November 25, 2014; revised January 26, 2015 and March 13, 2015; accepted April 3, 2015. Date of publication April 7, 2015; date of current version May 14, 2015. This work was supported by the National Natural Science Foundation of China under Grant 61176046, the International Science Technology Cooperation Program of China under Grant 2013DFR00730 and the Hundred Talents Program of Chinese Academy of Sciences.

The authors are with the State Key Laboratory of Luminescence and Application, Changchun Institute of Optics, Fine Mechanics and Physics, Chinese Academy of Sciences, 130033 Changchun, China (e-mail: tongcz@ciomp.ac.cn).

Color versions of one or more of the figures in this paper are available online at <http://ieeexplore.ieee.org>.

Digital Object Identifier 10.1109/JSTQE.2015.2420669

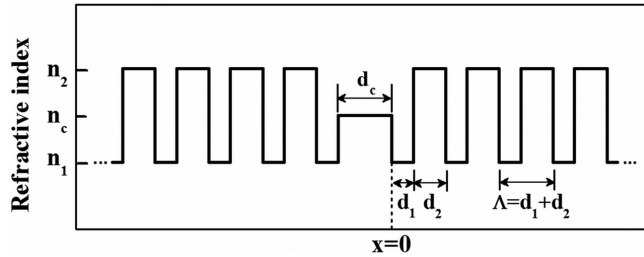


Fig. 1. Schematic diagram of the MBW.

However, these reported BRW lasers operate at leaky-mode with double-lobed FF. In this paper, we modified the BRW structure using the defect design of medium index to avoid the operation of conventional BRW leaky-mode. The edge-emitting diode lasers based on this modified Bragg-like waveguide (MBW) can realize an ultranarrow single-lobe FF. The stable circular beam with $\theta_{\perp, \text{FWHM}} < 5^\circ$, $\theta_{\perp, 95\%} < 10^\circ$ and watt-level power emission are demonstrated. The mechanism of this kind of diode lasers is present and the stability of FF is discussed. Finally, the detail information about the voltage characteristics, thermal properties and fiber coupling efficiency are also reported.

II. DEVICE DESIGN AND FABRICATION

A. Theoretical Model

The structure of MBW is schematically shown in Fig. 1. It consists of a mode-localized optical defect layer sandwiched between the top and bottom distributed Bragg reflector (DBR), which is made up of periodically alternated low and high index materials with index values of n_1 and n_2 , respectively. The active region is located in the defect layer.

The FF pattern of the laser is determined by the mode shape in the cavity [23]. There exists two regimes of PBG guidance, which are respectively $n_{\text{eff}} < n_1$ and $n_1 < n_{\text{eff}} < n_2$ [24]. Here, n_{eff} is the effective index of guided mode, n_1 and n_2 are respectively the low and high index of DBR. In the earlier reported BRW lasers, as the core defect layer has a lowest refractive index in the waveguide, the laser operates with $n_{\text{eff}} < n_1$. In this regime, light will propagate in all layers, leading to a NF intensity profile with periodic local maxima and nulls. This NF distribution can be approximated as a cosine function, resulting in a double-lobed FF [25]. If the core thickness is substantially increased, the NF profile would be confined only within the core layer, resulting in a single-lobed FF [26]. However, its FF angle is mainly dependent on the core thickness similarly with the conventional TIR waveguide, difficult to achieve ultranarrow beam divergence. Here, we utilized the core defect layer with a medium index, whose value is between the low and high index in one pair DBR. Through controlling the defect thickness, the effective index of the fundamental mode is ensured to be in the range $n_1 < n_{\text{eff}} < n_2$. In this case, light propagates ($n_{\text{eff}} < n_2$) in the layers with high index n_2 but is evanescent ($n_{\text{eff}} > n_1$) in the layers with low index n_1 . The NF distribution shows a Gaussian shaped envelope with very small amplitude

oscillations, whose FF pattern will be single-lobe. This method can also achieve large mode expansion and thus narrow beam divergence.

As shown in Fig. 1, the core defect layer has a refractive index n_c and thickness d_c . The thicknesses of low and high index n_1 and n_2 layers are respectively d_1 and d_2 , and the period is $\Lambda = d_1 + d_2$. Define the epitaxial direction as x axis. Assuming that the light wave propagates along the z -axis (in the direction of resonant cavity) and the waveguide is invariant in the y axis (the lateral direction of the device), the optical field distribution for the effective index in the range $n_1 < n_{\text{eff}} < n_2$ can be written as [27], [28]:

$$\varphi_y(x) = \begin{cases} a_c \exp(ik_c x) + b_c \exp(-ik_c x), & \text{for } -d_c < x \leq 0 \\ a_n \exp[-\gamma_1(x - n\Lambda)] + b_n \exp[\gamma_1(x - n\Lambda)], & \text{for } 0 < (x - n\Lambda) \leq d_1 \\ c_n \exp[ik_2(x - n\Lambda - d_1)] + d_n \exp[-ik_2(x - n\Lambda - d_1)], & \text{for } d_1 < (x - n\Lambda) \leq \Lambda \end{cases} \quad (1)$$

In this equation, a_n, b_n, c_n, d_n are the field amplitudes in the n th cell ($n = 0, 1, 2, \dots$, the zeroth cell is adjacent to the core defect layer). $\gamma_1 = k_0(n_{\text{eff}}^2 - n_1^2)^{1/2}$, is the decay factor of field amplitude in the low-index layer. $k_c = k_0(n_c^2 - n_{\text{eff}}^2)^{1/2}$ and $k_2 = k_0(n_2^2 - n_{\text{eff}}^2)^{1/2}$, represent the x component of the wave vector in the defect layer and high-index layer respectively. k_0 is the vacuum wave constant.

By imposing the boundary conditions (continuity of E and $\partial E / \partial x$ in the case of transverse-electric (TE) modes, or continuity of H and $(\partial H / \partial x)/n^2$ in the case of transverse-magnetic (TM) modes) at the interfaces $x = n\Lambda + d_1$ and $x = (n+1)\Lambda$. The transfer matrix between the vectors representing optical fields in two adjacent periods can be expressed as:

$$\begin{pmatrix} a_{n+1} \\ b_{n+1} \end{pmatrix} = \begin{pmatrix} T_{11} & T_{12} \\ T_{21} & T_{22} \end{pmatrix} \begin{pmatrix} a_n \\ b_n \end{pmatrix}. \quad (2)$$

The elements of the matrix are given as follows:

$$\begin{aligned} T_{11} &= \exp(-\gamma_1 d_1) \left[\cos k_2 d_2 - \frac{1}{2} \left(\frac{\gamma_1 K_1}{k_2} - \frac{k_2}{\gamma_1 K_1} \right) \sin k_2 d_2 \right], \\ T_{12} &= \exp(\gamma_1 d_1) \left[\frac{1}{2} \left(\frac{\gamma_1 K_1}{k_2} + \frac{k_2}{\gamma_1 K_1} \right) \sin k_2 d_2 \right], \\ T_{21} &= \exp(-\gamma_1 d_1) \left[-\frac{1}{2} \left(\frac{\gamma_1 K_1}{k_2} + \frac{k_2}{\gamma_1 K_1} \right) \sin k_2 d_2 \right], \\ T_{22} &= \exp(\gamma_1 d_1) \left[\cos k_2 d_2 + \frac{1}{2} \left(\frac{\gamma_1 K_1}{k_2} - \frac{k_2}{\gamma_1 K_1} \right) \sin k_2 d_2 \right] \end{aligned} \quad (3)$$

where $K_1 = 1$ for the TE mode and $K_1 = n_2^2/n_1^2$ for the TM mode.

Assume that the cladding layer on each side of the core layer contains an infinite number of periods, so the wave traveled in the periodic structure can be treated as Bloch wave. According to the Bloch formulation of electromagnetic wave propagation in a layered medium, the optical field can be described

by one periodic field in the following form, $\varphi(x, z) = \varphi_K(x)\exp(iKx)\exp(i\beta z)$. In this equation, K is the Bloch wave constant. Then the periodic condition can be expressed as:

$$\begin{pmatrix} a_{n+1} \\ b_{n+1} \end{pmatrix} = e^{iK\Lambda} \begin{pmatrix} a_n \\ b_n \end{pmatrix} = \begin{pmatrix} T_{11} & T_{12} \\ T_{21} & T_{22} \end{pmatrix} \begin{pmatrix} a_n \\ b_n \end{pmatrix}. \quad (4)$$

The phase factor $\exp(iK\Lambda)$ is the eigenvalue of this matrix and can be expressed by the following equation [28]:

$$\begin{aligned} e^{iK\Lambda} &= \\ &\frac{(T_{11} + T_{22}) \pm \sqrt{(T_{11} + T_{22})^2 - 4(T_{11} \cdot T_{22} - T_{12} \cdot T_{21})}}{2} \\ &= \chi \pm \sqrt{\chi^2 - 1}. \end{aligned} \quad (5)$$

From (5), K can be obtained by $K = \cos^{-1}(\chi)/\Lambda$ with $\chi = (T_{11} + T_{22})/2$. $|\chi| < 1$ corresponds to the real K and propagating Bloch wave. The condition $|\chi| \geq 1$ defines the forbidden bands of the periodic medium, where K has an imaginary part. The eigenvectors corresponding to the above eigenvalues (5) are given by

$$\begin{pmatrix} a_n \\ b_n \end{pmatrix} = e^{inK\Lambda} \begin{pmatrix} a_0 \\ b_0 \end{pmatrix} = Ce^{inK\Lambda} \begin{pmatrix} T_{12} \\ e^{iK\Lambda} - T_{11} \end{pmatrix}, \quad (6)$$

where C is an arbitrary constant.

By applying the continuity condition at the core-cladding interface ($x = 0$), the field amplitudes in the defect layer can be related to those in the first cladding low-index layer as:

$$\begin{pmatrix} a_c \\ b_c \end{pmatrix} = \frac{1}{2} \begin{pmatrix} 1 + \frac{iK_g\gamma_1}{k_c} & 1 - \frac{iK_g\gamma_1}{k_c} \\ 1 - \frac{iK_g\gamma_1}{k_c} & 1 + \frac{iK_g\gamma_1}{k_c} \end{pmatrix} \begin{pmatrix} a_0 \\ b_0 \end{pmatrix}, \quad (7)$$

where $K_g = 1$ for the TE mode and $K_g = (n_c/n_1)^2$ for the TM mode.

The guided modes of such waveguide should satisfy the transverse resonance condition [28]:

$$2k_c d_c + 2\phi_c = 2m_b \pi \quad \text{for } m_b = 0, 1, 2, \dots \quad (8)$$

where ϕ_c is the phase shift acquired at the boundary between the defect layer and low-index layer, and the integer m_b is the mode order. The reflectance at $x = 0$ can be obtained from (6) and (7) as $R = b_c/a_c$. As in the photonic bandgap, the amplitude reflection coefficient from the semi-infinite DBR cladding is 1, and the reflected wave acquires only a phase shift ϕ_c . Therefore, the reflection phase ϕ_c can be obtained from $R = \exp(i\phi_c)$ [28]. From (8), the mode dispersion curves or the propagation constants of the guided modes can be obtained.

In this paper, the gain material is GaAs_{0.86}P_{0.14} quantum well (QW) emitting at 808 nm, which is placed at the center of the defect layer. Owing to the large tensile-strain ($\varepsilon = 0.5\%$) in the active region, the lasing emission is TM polarized. The top and bottom DBR is made up of 100 nm Al_{0.35}Ga_{0.65}As and 600 nm Al_{0.5}Ga_{0.5}As. To make sure that the effective index of guided modes is located in the range of $n_1 < n_{\text{eff}} < n_2$, the calculated dispersion curves for 250 nm thick Al_{0.3}Ga_{0.7}As defect layer are shown in Fig. 2(a). The shaded region indicates that the

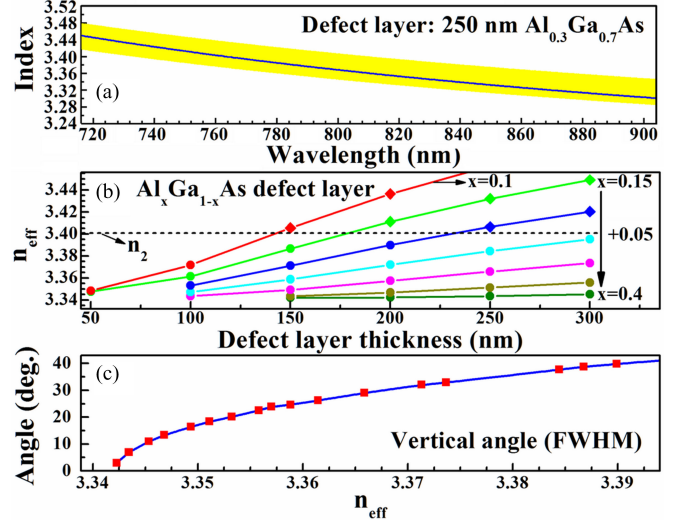


Fig. 2. (a) The dispersion curves for the MBW with 250 nm thick Al_{0.3}Ga_{0.7}As defect layer, (b) the effective index of fundamental mode at 808 nm with the Al_xGa_{1-x}As defect layer, (c) calculated vertical divergence angle, θ_{FWHM} , as a function of the effective index of guided mode.

effective index n_{eff} satisfies the condition of single-lobed FF, and the dashed lines inside corresponds to the effective index when $m_b = 0$. For such defect layer of 250 nm Al_{0.3}Ga_{0.7}As, there is only one guided mode within the range of $n_1 < n_{\text{eff}} < n_2$.

The characteristics of defect layer will affect obviously the effective index of guided modes. Fig. 2(b) plots the effective index of the fundamental mode at 808 nm for the defect layer of Al_xGa_{1-x}As (x is from 0.1 to 0.4). As can be seen, with the increase in refractive index and thickness of the defect layer, the effective index of guided mode will increase, the dispersion curve of fundamental mode will move upward and more modes can be guided in the waveguide. However, for a thick enough defect layer with a high refractive index, e.g., 200 nm Al_{0.1}Ga_{0.9}As, the optical field of the fundamental mode will be confined mainly by the index-guiding effect rather than PBG guiding with $n_{\text{eff}} > n_2$. Note that the effective index will affect the decay rate of field amplitude in the low-index layer and hence determine the FF angle, where the field magnitude will vary slowly when the effective index is sufficiently close to the value of n_1 . When the Al-content of defect layer increases to 0.45, the dispersion curves will be terminated at the edges and the corresponding guided modes are cut off, leading to the BRW mode with $n_{\text{eff}} < n_1$. Fig. 2(c) shows the dependence of the FWHM divergence angle on the effective index of such waveguide. It shows that compressing the effective index of guided mode tends to significantly reduce the FF angle. When the effective index of mode is near to the optimized value, the FF angle will reduce from 40° to less than 5° quickly. Therefore, to obtain a low divergence angle, the refractive index and thickness of defect layer have to be decreased to allow only one guided mode and $n_1 < n_{\text{eff}} < n_2$.

Although the expanded optical field can improve the FF characteristics, it will also cause the low optical confinement factor (OCF) and hence the low modal gain in the diode laser.

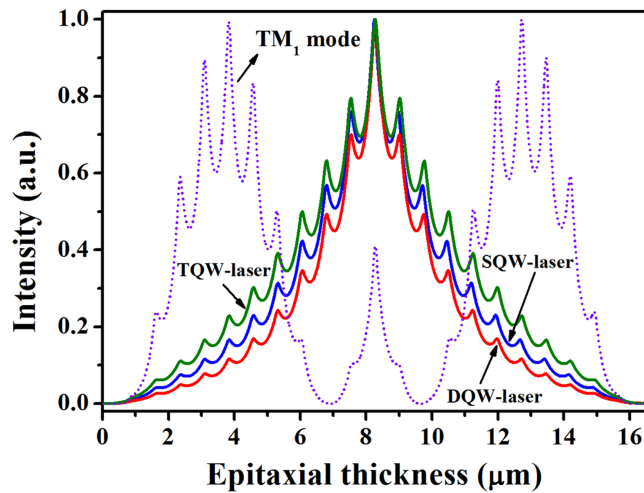


Fig. 3. Calculated vertical NF distribution of the fundamental mode TM_0 of SQW-laser (blue line), DQW-laser (red line) and TQW-laser (green line), the dashed line shows the NF distribution of high-order TM_1 mode.

Increasing the QW number is helpful to achieve high output power. However, the refractive index of QW material is usually much higher than that of the surrounding waveguide layer. The wave-guiding due to the QW active region itself will limit the minimum achievable FF angle especially for the wide waveguide laser [12]. Therefore, how to increase the output power while maintaining low divergence angle is a key issue for the laser design with MBW. To obtain the large optical mode extension in multi-QW laser, the strength of localization for the light from the optical defect should be reduced, which can ensure that the n_{eff} approaches the low index n_1 in the DBR regions, and leads to an enlarged spot size but without dramatic decrease in the OCF for the fundamental mode. In this paper, the medium-index $\text{Al}_{0.4}\text{Ga}_{0.6}\text{As}$ material is used as the defect layer to reduce the beam divergence. In order to find the optimized condition for the high power and narrow vertical FF angle simultaneously, we designed the laser structures with single QW (SQW), double QWs (DQW) and triple QWs (TQW). For the laser with SQW, a 110 nm thick $\text{Al}_{0.4}\text{Ga}_{0.6}\text{As}$ defect layer was chosen. If the QW number is increased to two without changing other layer parameters, the optical mode will be stronger confined in the defect layer, resulting in about 5° increase of the beam divergence. Therefore, we reduce the thickness of $\text{Al}_{0.4}\text{Ga}_{0.6}\text{As}$ defect layer to 80 nm for the laser with DQW so as to keep the divergence angle unchanged. The $\text{Al}_{0.4}\text{Ga}_{0.6}\text{As}$ layer thickness of the laser with TQW is substantially reduced to 40 nm for further reduction of the vertical beam divergence.

Fig. 3 shows the calculated NF intensity profiles of the fundamental TM mode and the adjacent high-order mode in these three lasers. It can be seen that these three laser structures have a similar NF profile except the different extent of mode expansion. The TM_0 mode is localized with its maximum in the defect layer and decays away from it, whereas the TM_1 mode and other high-order modes are extended over the entire waveguide and penetrate into the substrate and the contact layer. This will result in significant losses and low modal gain for the high-order

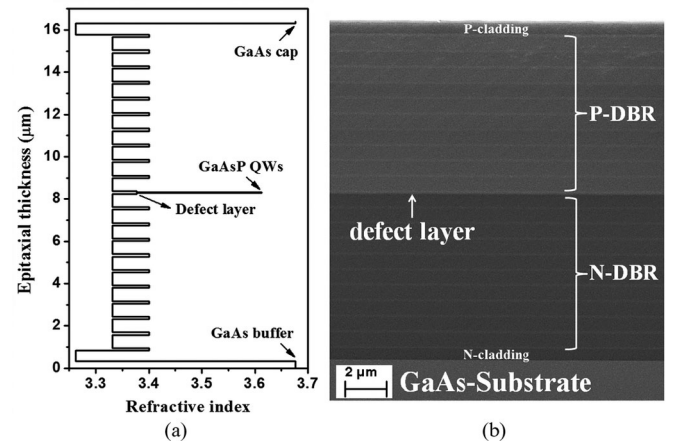


Fig. 4. (a) Distribution of refractive index in the laser with MBW. (b) The cross-sectional SEM micrograph of the laser wafer.

modes. Therefore, the designed laser can operate under the single transverse mode. The TQW-laser shows the largest optical mode size due to the significantly reduced thickness of defect layer, which reflects that the decrease in the thickness of defect layer can restrain the localized optical waveguide effect of high index QW region and maintain narrow beam divergence. The calculated OCF for the SQW, DQW and TQW lasers are 0.27%, 0.69%, and 0.63%, respectively.

B. Device Fabrication

The laser structure was grown on (100)-oriented, n⁺ GaAs substrate by Aixtron-200 metal-organic chemical vapour deposition (MOCVD). All DBR interfaces were linearly graded in composition of 20 nm to reduce the electrical resistance. The doping profile is carefully adjusted to reduce the internal loss. The refractive index distribution of the designed laser is shown in Fig. 4(a), and the total thickness of epitaxial layers exceeds 16 μm. Fig. 4(b) shows the cross-sectional scanning electron microscope (SEM) micrograph of the grown laser structure, which reveals clearly the defect layer, top and bottom DBR.

After the growth, the samples were patterned into broad area stripe lasers with the width of 150 μm by photolithography and etching. To investigate the influence of etching depth on the FF stability and emission power, the stripes with two different depths were fabricated for the SQW-laser. One is 1 μm depth defined by wet etching and called as shallow stripe, the other is 6 μm depth formed by dry etching and named as deep stripe. The etching depths for DQW and TQW laser are about 6 μm, which means the top Bragg reflector is almost etched out completely. 350-nm SiO₂ was deposited as the electrical insulating layer, a contact window opening was defined and etched, followed by the standard p-side metallization. Finally, after the substrate thinning and n-side metallization, the diode lasers were cleaved into single devices without any passivation or coating. In the measurement, the unmounted laser chips were placed on copper heat-sinks with p-side down and the electrical potential is applied through a thin metal needles contacted to the n-side metal

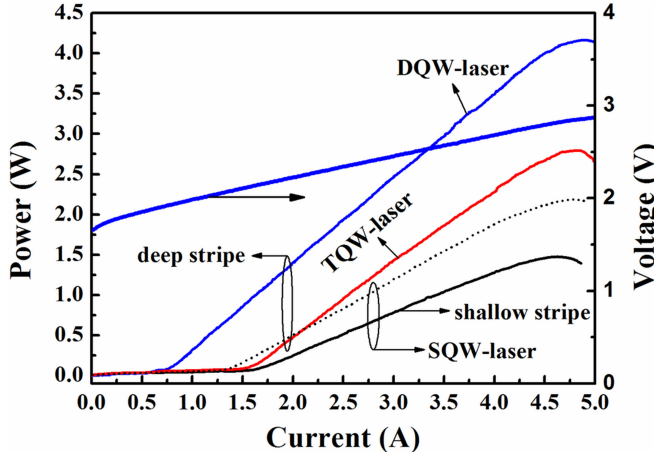


Fig. 5. L - I - V characteristics of the lasers with various QW number.

contact. For further characterizing the designed lasers, we fabricated $90\text{ }\mu\text{m}$ -wide DQW-laser coated with high-reflective (HR) and anti-reflective (AR) facet coating, which were soldered p-side down on CuW submount.

III. EXPERIMENTAL RESULTS AND DISCUSSION

A. Output Power and QW Numbers

Fig. 5 plots the measured light-current-voltage (L - I - V) characteristics of the unmounted lasers ($150\text{-}\mu\text{m}$ -wide, $1400\text{-}\mu\text{m}$ -long) under quasi-continuous-wave (QCW, $200\text{ }\mu\text{s}$ pulses of 200 Hz frequency) operation at room temperature. It can be seen that the laser with two QWs shows the lowest threshold current of 0.74 A and the highest slope efficiency of 1.06 W/A . The maximum output power is 4.2 W without any catastrophic optical damage phenomena before the onset of thermal roll-over. The TQW-laser reveals a higher threshold current of 1.53 A and lower output power of 2.8 W compared with the DQW-laser. This might be resulted from the increased absorption loss caused by the significantly enlarged optical mode.

Etching depth shows its obvious influence on the emission power. The threshold current for the SQW-laser with shallow stripe is about 1.6 A , and the maximum optical power is 1.47 W . On the contrary, deep etching reduces the threshold current down to 1.3 A , and the emission power reaches 2.1 W , which is contributed from the reduced carrier diffusion and leakage in the lateral direction due to the deep stripe. The following FF results also demonstrated the compressing of lateral carrier diffusion plays an important role on the stability of lateral FF angle. The maximum output powers of these samples were all limited by the thermal rollover due to the poor heat conduction in the tested devices without soldering and packaging. The deep-etched lasers with different QW numbers have nearly the same voltage characteristics. The measured series resistance for these devices is about $230\text{ m}\Omega$. This relatively high resistance might result from the multiple reverse biased hetero-junctions and extra contact resistance for the unmounted devices.

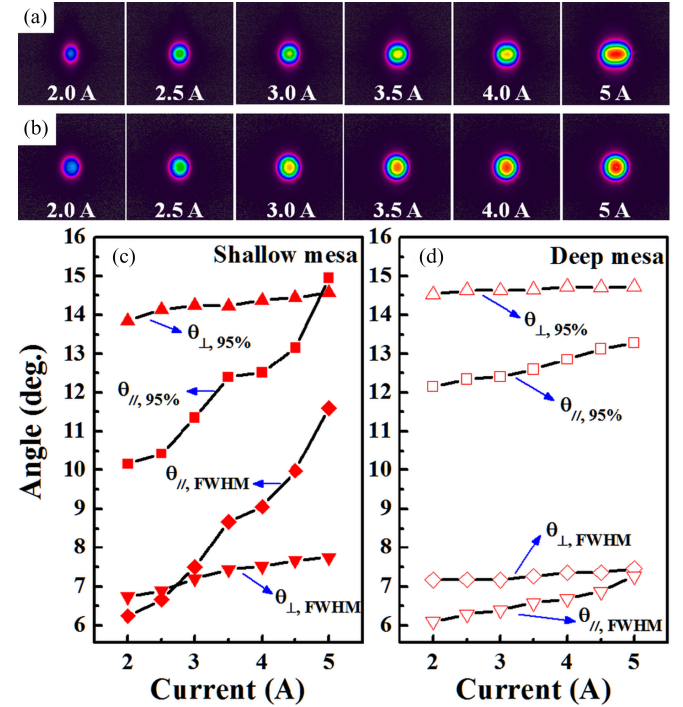


Fig. 6. Measured FF spot patterns at various currents of SQW-laser with (a) shallow and (b) deep stripe; (c) and (d) are the corresponding FF angle with shallow and deep mesa, respectively.

B. Far-Field Characteristics and Stability

To characterize the FF and investigate stability of the fabricated lasers, the FF patterns and profiles are measured. Fig. 6 shows the measured FF spot patterns of the SQW-laser with shallow stripe (see Fig. 6(a) and (c)) and deep-etched stripe (see Fig. 6(b) and (d)) at different injection currents. The devices show the nearly circular emission spots with ultralow divergence. The FF spots of shallow stripe devices reveal an evidently broaden in the lateral direction with the increase of injection current, which might be attributed to the current-induced thermal lensing due to the serious lateral current diffusion in the shallow etched stripe [29]. On the contrary, when utilizing deep and steep stripe to suppress lateral current leakage, the laser shows a much more stable lateral FF and nearly circular spot for all the injected currents as shown in Fig. 6(b), indicating that the deep stripe is beneficial to improve the lateral beam quality. Although the laser operates under multi-lateral-mode, the obvious beam filamentation could not be seen even at high injected current, which might be because that the large vertical mode extension leads to a low modal gain and thus reduce the generation possibility of beam filamentation [16]. Fig. 6(c) and (d) show the quantitative results on the dependence of vertical and lateral divergence angles of the SQW-laser on the injected current shown in Fig. 6(a) and (b). Two kinds of definitions on the divergence angle, 95% power content and FWHM definition, are both shown. As can be seen, the FF angle in the vertical direction is almost independent on the current for both devices. The vertical divergence angle of the shallow-etched SQW-laser

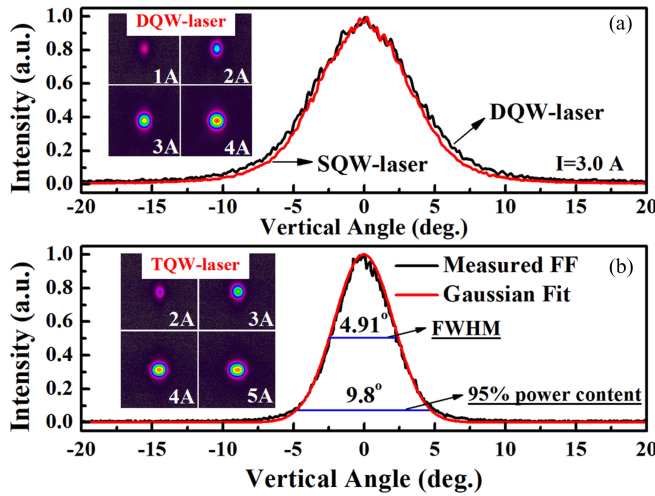


Fig. 7. (a) Measured vertical FF distribution at 3 A current of the SQW and DQW laser, the inset shows measured FF spots of the DQW-laser at various currents; (b) measured and Gaussian-fit vertical FF distribution of the TQW-laser, the inset shows measured FF spots of the TQW-laser.

is 6.7° ($\theta_{\perp,\text{FWHM}}$) and 13.8° ($\theta_{\perp,95\%}$) at 2 A and increase no more than 1° at the current of 5 A. However, the lateral FF divergence angle $\theta_{\parallel,\text{FWHM}}$ broadens rapidly from 6.2° to 11.6° and the $\theta_{\parallel,95\%}$ increases from 10.1° to 15.4° . The aspect ratio of the FF pattern is below 2 in the whole operating range. On the other hand, the deep mesa device exhibits a nearly unchanged vertical FF divergence of 7.1° ($\theta_{\perp,\text{FWHM}}$) and 14.5° ($\theta_{\perp,95\%}$). The sensitivity of lateral divergence on the operation current reduces significantly, which is about 6.1° ($\theta_{\parallel,\text{FWHM}}$) at 2 A and increases to 7° at 5 A. The corresponding values of $\theta_{\parallel,95\%}$ are respectively 12.1° and 13° , which reveals a very stable circular beam output with the aspect ratio close to 1 until the highest current.

Fig. 7 shows the measured FF profiles of the DQW-laser and TQW-laser in vertical direction, which are near Gaussian distributions. In Fig. 7(a), it reveals the $\theta_{\perp,\text{FWHM}}$ of 8.1° at 3 A for the DQW-laser, which is slightly higher than that of SQW-laser. The behind reason is because of the reduced mode size as shown in Fig. 3. As shown in the inset of Fig. 7(a), the DQW-laser exhibits a stable circular beam output for the current above 3 A. In Fig. 7(b), it shows a perfectly Gaussian-shaped vertical FF profile of the TQW-laser at 2.25 A and the corresponding $\theta_{\perp,\text{FWHM}}$ and $\theta_{\perp,95\%}$ are respectively as low as 4.91° and 9.8° , being considerably narrower than that of commercial diode lasers. It was worth to note that the TQW-laser achieves the lowest vertical FF divergence, proving that the significant expansion of optical field can also be achieved for multi-QW laser through reducing the thickness and index of defect layer.

Fig. 8 shows the stability of FF divergence of TQW-laser at different injection currents. The vertical FF angle θ_\perp is very stable, only 0.85° increase for the FWHM definition with the current increasing from 2 to 5 A. The corresponding variation of $\theta_{\perp,95\%}$ is from 9.7° to 11.2° , which is about 5% expansion with per ampere current injection. The lateral FF angle shows

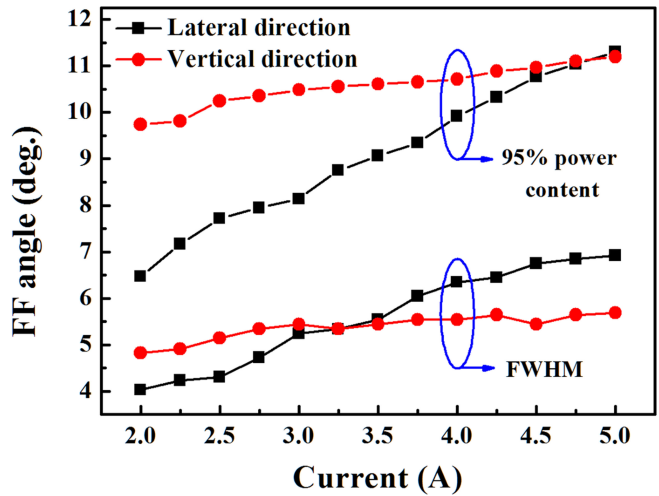


Fig. 8. FF stability of TQW-laser in the vertical direction (filled circles) and lateral direction (filled squares).

a relatively sensitive dependence on the injection current, but their values are still low. $\theta_{\parallel,\text{FWHM}}$ is 4° at 2 A and increases to 6.9° at 5 A. The corresponding $\theta_{\parallel,95\%}$ are respectively 6.5° and 11.3° at 2 and 5 A. The $\theta_{\parallel,95\%}$ and $\theta_{\perp,95\%}$ are same at 4.8 A, which reveals a circular emission beam with an angle of 11.1° . For the FWHM definition of FF angle, the perfect circular beam corresponds to the angle of 5.3° . In the broad area lasers, the increasing current results in the onset of a large number of lateral modes, degrading the FF angle [29]. Due to the rapidly changed lateral divergence but stable vertical divergence, the circular beam behavior observed for these device occurs only at a narrow range of bias currents. The aspect ratio of vertical direction versus lateral direction first reduces from 1.2 at 2 A to 1 at 3.25 A, then reduces to 0.82 at 5 A. Therefore, in order to achieve stable circular beam behavior, single lateral mode operation is important [18]. This needs lateral mode control, such as utilizing ridge waveguide, tapered structure or the lateral gratings.

C. Characteristics of Packaged Devices

For continuous-wave (CW) measurements, we fabricated $90 \mu\text{m}$ -wide and 4 mm-long DQW-laser device with deep-etched stripe. The devices were coated with AR/HR facet coating and then soldered p-side down on CuW submount with AuSn solder. Fig. 9 depicts the L - I - V characteristics from 10°C to 20°C (heat-sink temperature) under CW test conditions. At 10°C , the threshold current is 1.5 A, and the maximum CW power exceeds 4.6 W at 10 A, limited by thermal rollover. The threshold current increases to 1.57 A at 20°C . The highest power at 15 and 20°C are respectively 4.5 and 4.2 W. The slope efficiencies are 0.77, 0.74 and 0.69 W/A when temperature varies from 10 to 20°C . The reduced slope efficiency is due to that the increased cavity length leads to a smaller relation of mirror loss to the total loss. The turn-on voltage is 1.54 V, approximately equivalent to the emission wavelength of the device. The measured series differential resistance $R_s \approx 45 \text{ m}\Omega$, which gives a resistivity of $16.2 \text{ m}\Omega\cdot\text{mm}^2$. The further improvement

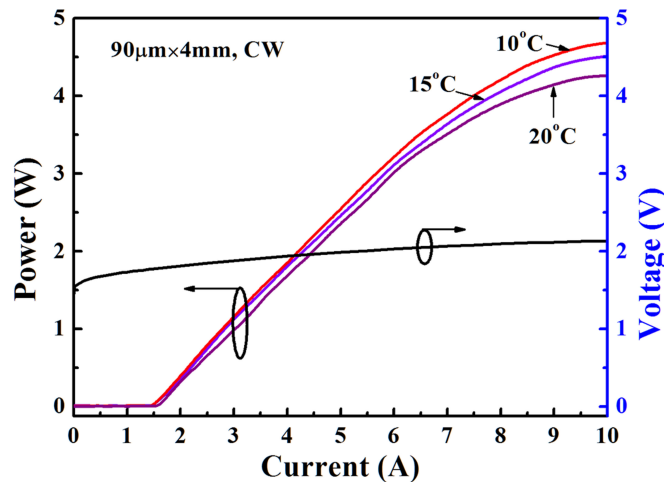


Fig. 9. Light-current-voltage (L - I - V) characteristics of the DQW-laser in CW mode at different temperatures.

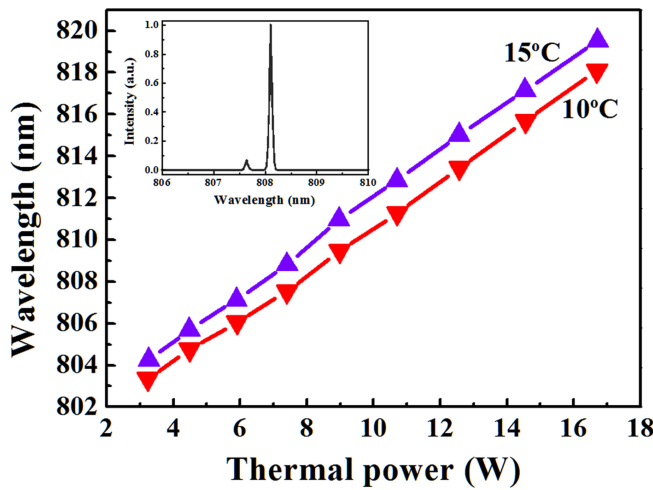


Fig. 10. The lasing wavelength versus wasted power at 10 and 15 °C, the inset shows the measured lasing spectrum at 3 W emission power.

of the series resistance can be achieved using the bandgap engineering methods to eliminate the band-discontinuity, such as parabolically graded interface [30], delta doping [31], and adding superlattices [32] at the interfaces of DBR.

The thermal resistance of the device was estimated by measuring the wavelength shift with current. The optical spectrum is measured as a function of the electrical power at a fixed heat-sink temperature of 10 °C and 15 °C. Increasing the pumping current, the wavelength will be red-shift. The heat dissipation power can be described as the total electrical power minus the output optical power. Fig. 10 shows the lasing wavelength shift versus the thermal power, which exhibits a linear behavior with coefficient of 1.1 nm/W. In the fabricated lasers, the temperature dependence of the modal gain peak is measured to be ~ 0.29 nm/K. Then the extracted thermal resistance is determined to be 3.8 K/W. The inset of Fig. 10 shows the measured lasing spectrum by an AQ6370C optical spectrum analyzer at 3 W output power. The central wavelength is 808.1 nm. The device

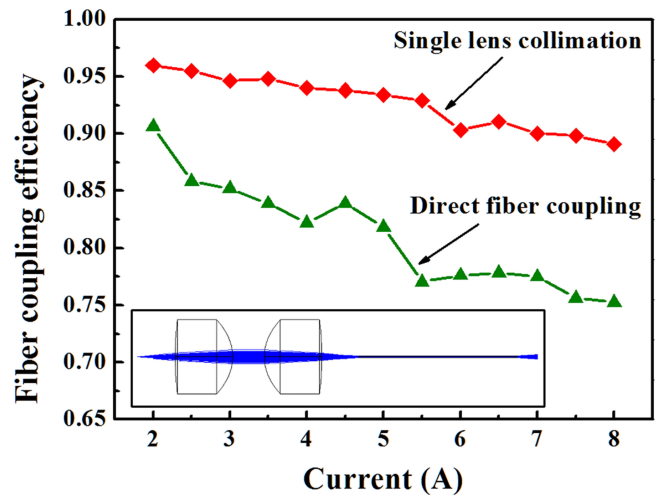


Fig. 11. The fiber coupling efficiency of the laser based on MBW at different currents, the inset shows the optical system for the method of single lens collimation.

operates in multi-longitudinal mode but with a very narrow spectral linewidth (FWHM) of ~ 0.1 nm.

The narrow circular beam emission of the laser with MBW is very promising to develop a low-cost coupling scheme into a fiber without complicated beam shaping. It allows to use lower NA fibers and collimation lenses with large focal length, reducing the tolerance of alignment. To test the fiber coupling efficiency, we used two methods to couple the output light into a normal commercial fiber (105 μ m core, NA = 0.15). The alignment process was carried out under 2 A current, and then the power in the fiber was measured under various currents without changing the lenses and fiber position. The first method is to couple the light directly into the fiber without utilizing any lenses or wedge-fiber. As shown in Fig. 11, a maximum coupling efficiency of 90.6% is achieved for this configuration, and the coupling efficiency degrades to 75% at 8 A. In the other method, the output light is first collimated by a commercial aspheric lens (focal length ~ 4.5 mm) and then imaged by a same lens on the fiber core, not employing the typical fast- and slow-axis respective collimation for conventional diode laser. The inset of Fig. 11 shows the optical setup and the simulated beam propagation by ZEMAX. A fiber coupling efficiency as high as 96% is obtained under 2 A. At higher pump current, the fiber coupling efficiency remains above 89%. For comparison, a similar arrangement using a conventional diode laser yielded a maximum coupling efficiency of only 42% and 67% respectively for these two methods.

IV. CONCLUSION

In summary, we had demonstrated the low divergence and circular beam emission from the edge-emitting diode lasers using the MBW, which overcome the drawbacks of traditional diode lasers. The broad area lasers emitting in 808 nm wavelength show a lowest vertical divergence of $< 5^\circ$ and $< 10^\circ$ in FWHM and 95% power content definitions, respectively. It presents the stable FF characteristics with Gaussian distributions

even at the highest operating current. It was found that reducing the index and thickness of the defect layer can improve the vertical divergence. The lateral divergence can be controlled by the deeply etched stripe. The packaged device with 90- μm -wide stripe achieved 4.6 W output power under CW operation. The narrow circular beam emission from the laser can greatly improve the fiber coupling efficiency without complicated beam shaping. We believe that our work will contribute to the development of low divergence diode lasers.

REFERENCES

- [1] B. C. Qiu, S. D. McDougall, X. F. Liu, G. Bacchin, and J. Marsh, "Design and fabrication of low beam divergence and high kink-free power lasers," *IEEE J. Quantum Electron.*, vol. 41, no. 9, pp. 1124–1130, Sep. 2005.
- [2] N. G. Basov, *Semiconductor Lasers* (Nobel lectures in Physics 1963–1970). Singapore: World Scientific Publishing, 1998, pp. 103–108.
- [3] A. Pietrzak, H. Wenzel, G. Erbert, and G. Tränkle, "High-power laser diodes emitting light above 1100 nm with a small vertical divergence angle of 13°," *Opt. Lett.*, vol. 33, no. 19, pp. 2188–2190, Oct. 2008.
- [4] A. Malag *et al.*, "Asymmetric heterostructure with reduced distance from active region to heatsink for 810-nm range high-power laser diodes," *IEEE J. Quantum Electron.*, vol. 48, no. 4, pp. 465–471, Apr. 2012.
- [5] J. X. Zhang *et al.*, "Large spot size and low-divergence angle operation of 917-nm edge-emitting semiconductor laser with an asymmetric waveguide structure," *Chin. Opt. Lett.*, vol. 10, no. 6, pp. 061401-1–061401-3, 061401, Jun. 2012.
- [6] C. T. Hung and T. C. Lu, "830-nm AlGaAs-InGaAs graded index double barrier separate confinement heterostructures laser diodes with improved temperature and divergence characteristics," *IEEE J. Quantum Electron.*, vol. 49, no. 1, pp. 127–132, Jan. 2013.
- [7] B. F. Cui *et al.*, "A tunnel regenerated coupled multi-active-region large optical cavity laser with high quality beam," *Chin. Phys. B*, vol. 21, no. 9, pp. 094209-1–094209-4, Sep. 2012.
- [8] G. W. Yang *et al.*, "High-performance 980-nm ridge waveguide lasers with a nearly circular beam," *IEEE Photon. Technol. Lett.*, vol. 16, no. 4, pp. 981–983, Apr. 2004.
- [9] B. Ma, S. Cho, C. Lee, Y. Kim, and Y. Park, "High-power 660-nm GaInP-AlGaInP laser diodes with low vertical beam divergence angles," *IEEE Photon. Technol. Lett.*, vol. 17, no. 7, pp. 1375–1377, Jul. 2005.
- [10] W. L. Li, Y. K. Su, S. J. Chang, and C. Y. Tsai, "A novel waveguide structure to reduce beam divergence and threshold current in GaInP/AlGaInP visible quantum-well lasers," *Appl. Phys. Lett.*, vol. 71, no. 16, pp. 2245–2247, Oct. 1997.
- [11] P. Crump *et al.*, "975 nm high power diode lasers with high efficiency and narrow vertical far field enabled by low index quantum barriers," *Appl. Phys. Lett.*, vol. 96, no. 13, pp. 131110-1–131110-3, Mar. 2010.
- [12] A. Pietrzak *et al.*, "Combination of low-index quantum barrier and super large optical cavity designs for ultranarrow vertical far-fields from high-power broad-area lasers," *IEEE J. Sel. Topics Quantum Electron.*, vol. 17, no. 6, pp. 1715–1722, Nov./Dec. 2011.
- [13] P. Yeh, A. Yariv, and C. S. Hong, "Electromagnetic propagation in periodic stratified media—Part I: General theory," *J. Opt. Soc. Amer.*, vol. 67, no. 4, pp. 423–438, Apr. 1977.
- [14] W. Liang, Y. Xu, J. M. Choi, and A. Yariv, "Engineering transverse Bragg resonance waveguides for large modal volume lasers," *Opt. Lett.*, vol. 28, no. 21, pp. 2079–2081, Nov. 2003.
- [15] M. V. Maximov *et al.*, "Narrow vertical beam divergence laser diode based on longitudinal photonic band crystal waveguide," *Electron. Lett.*, vol. 39, no. 24, pp. 1729–1731, Nov. 2003.
- [16] M. V. Maximov *et al.*, "High-Power low-beam divergence edge-emitting semiconductor lasers with 1- and 2-D photonic bandgap crystal waveguide," *IEEE J. Sel. Topics Quantum Electron.*, vol. 14, no. 4, pp. 1113–1122, Jul./Aug. 2008.
- [17] T. Kettler *et al.*, "High-brightness and ultranarrow-beam 850-nm GaAs/AlGaAs photonic band crystal lasers and single-mode arrays," *IEEE J. Sel. Topics Quantum Electron.*, vol. 15, no. 3, pp. 901–908, May/Jun. 2009.
- [18] I. I. Novikov *et al.*, "High-power single mode (>1 W) continuous wave operation of longitudinal photonic band crystal lasers with a narrow vertical beam divergence," *Appl. Phys. Lett.*, vol. 92, no. 10, pp. 103515-1–103515-3, Mar. 2008.
- [19] L. Liu *et al.*, "Design and analysis of laser diodes based on the longitudinal photonic band crystal concept for high power and narrow vertical divergence," *IEEE J. Sel. Topics Quantum Electron.*, vol. 21, no. 1, pp. 1900107-1–1900107-7, Jan./Feb. 2015.
- [20] G. Erbert *et al.*, "High brightness diode lasers with very narrow vertical divergence," *Proc. SPIE*, vol. 6909, pp. 69090P-1–69090P-11, Jan. 2008.
- [21] B. J. Bijlani and A. S. Helmy, "Bragg reflection waveguide diode lasers," *Opt. Lett.*, vol. 34, no. 23, pp. 3734–3736, Dec. 2009.
- [22] C. Z. Tong, B. Bijlani, S. Alali, and A. S. Helmy, "Characteristics of edge emitting Bragg reflection waveguide lasers," *IEEE J. Quantum Electron.*, vol. 46, no. 11, pp. 1605–1610, Nov. 2010.
- [23] L. J. Wang *et al.*, "High power single-sided Bragg reflection waveguide lasers with dual-lobed far field," *Appl. Phys. B*, vol. 107, no. 3, pp. 809–812, Jun. 2012.
- [24] R. F. Cregan *et al.*, "Single-mode photonic band gap guidance of light in air," *Science*, vol. 285, no. 5433, pp. 1537–1539, Sep. 1999.
- [25] L. J. Wang *et al.*, "Bragg reflection waveguide twin-beam lasers," *Laser Phys.*, vol. 23, no. 10, pp. 105802-1–105802-5, Oct. 2013.
- [26] N. Zareian, P. Abolghasem, and A. S. Helmy, "Far field of Bragg reflection waveguides: Characteristics and closed-form approximation," *J. Lightw. Technol.*, vol. 29, no. 5, pp. 728–735, Mar. 2011.
- [27] B. R. West and A. S. Helmy, "Properties of the quarter-wave Bragg reflection waveguide: Theory," *J. Opt. Soc. Amer. B.*, vol. 23, no. 6, pp. 1207–1220, Jun. 2006.
- [28] J. Li and K. S. Chiang, "Analysis of one-dimensional high-index guiding photonic bandgap waveguides," *J. Opt. Soc. Amer. B.*, vol. 26, no. 11, pp. 2007–2015, Nov. 2009.
- [29] P. Crump *et al.*, "Experimental and theoretical analysis of the dominant lateral waveguiding mechanism in 975 nm high power broad area diode lasers," *Semicond. Sci. Technol.*, vol. 27, no. 4, pp. 045001-1–045001-9, Apr. 2012.
- [30] E. F. Schubert *et al.*, "Elimination of heterojunction band discontinuities by modulation doping," *Appl. Phys. Lett.*, vol. 60, no. 4, pp. 466–468, Jan. 1992.
- [31] K. L. Leara and P. R. Schneider, "Uniparabolic mirror grading for vertical cavity surface emitting lasers," *Appl. Phys. Lett.*, vol. 68, no. 5, pp. 605–607, Jan. 1996.
- [32] K. Kurihara *et al.*, "Reduction in the series resistance of the distributed Bragg reflector in vertical cavities by using quasi-graded superlattices at the heterointerfaces," *J. Appl. Phys.*, vol. 73, no. 1, pp. 21–27, Jan. 1993.

Lijie Wang received the B.S. degree in optical communications from Jilin University, Changchun, China, in 2008. He received the Ph.D. degree in condensed matter physics from the Changchun Institute of Optics, Fine Mechanics and Physics, Chinese Academy of Sciences, Changchun, China, in 2013, where he is currently working as a Research Associate.

His current research interests include high brightness diode lasers, mid-infrared lasers, and photonic crystal lasers.

Cunzhu Tong (M'09) received the B.S. and M.S. degrees in physics from Chongqing University, Chongqing, China, and the Ph.D. degree in microelectronics and solid electronics from the Institute of Semiconductors, Chinese Academy of Sciences, Beijing, China.

He was a Research Fellow with Nanyang Technological University, Singapore, from 2005 to 2009. After that, he joined the Department of Electrical and Computer Engineering, University of Toronto, Toronto, ON, Canada, as a Postdoctoral Researcher. He became a Professor of Hundred Talents Program in CAS and was with the Changchun Institute of Optics, Fine Mechanics and Physics, Chinese Academy of Sciences, Changchun, China, in November 2010. He has authored and coauthored more than 60 refereed journal and conference papers, and has presented numerous invited talks and tutorials. His current research interests include Bragg reflection waveguide devices, photonic crystal lasers, mid-infrared lasers, and beam combining of diode lasers.

Sicong Tian received the B.S. degree and Ph.D. degrees in physics from Jilin University, Changchun, China, respectively, in 2007 and 2012.

He is currently a Research Associate with the State Key Laboratory of Luminescence and Application, Changchun Institute of Optics, Fine Mechanics and Physics, Chinese Academy of Sciences, Changchun, China. His current research interests include quantum optics, quantum dot, and photonic crystal.

Shili Shu received the received the B.S. and Ph.D. degrees in materials from Jilin University, Changchun, China, respectively, in 2008 and 2013.

He joined Changchun Institute of Optics, Fine Mechanics and Physics, Chinese Academy of Sciences, Changchun, China, in 2013. His current research interests include diode laser packaging and heat pipe.

Yugang Zeng received the B.S. degree from the Department of Material Science and Engineering, Tsinghua University, Beijing, China, in 2002, and the Ph.D. degree in microelectronics and solid electronics from the Institute of Semiconductors, Chinese Academy of Sciences, Changchun, China.

He joined the Changchun Institute of Optics, Fine Mechanics and Physics in 2008. His current research interests include III-V MOCVD epitaxy and high power vertical-cavity surface-emitting lasers.

Jiamin Rong received the B.S. degree in physics from Guizhou University, Guiyang, China, in 2011. She is currently working toward the Ph.D. degree in condensed matter physics at the Changchun Institute of Optics, Fine Mechanics and Physics, Chinese Academy of Sciences, Changchun, China.

Her current research interests include the GaSb-based diode lasers.

Hao Wu received the B.S. degree from the University of Science and Technology of China, Hefei, China, in 2007. He received the Ph.D. degree from the Institute of Semiconductors, Chinese Academy of Sciences, Beijing, China, in 2012.

He joined the Changchun Institute of Optics, Fine Mechanics and Physics in 2012. His current research interests include beam transform and coupling of mid-infrared diode lasers.

Enbo Xing received the B.S. degree from Jilin University, Changchun, China, and he is currently working toward the Ph.D. degree in condensed matter physics at the Changchun Institute of Optics, Fine Mechanics and Physics, Chinese Academy of Sciences, Changchun, China.

His current research interests include photonic crystal laser.

Yongqiang Ning received the M.S. degree in semiconductor materials from Beijing General Research Institute for Nonferrous Metals, Beijing, China, in 1990, and the Ph.D. degree in condensed matter physics from the Changchun Institute of Optics, Fine Mechanics and Physics, Chinese Academy of Sciences, Changchun, China, in 1999.

He was a Visiting Scholar with Cardiff University, Wales, U.K., from 1999 to 2000. He is currently a Professor with the Changchun Institute of Optics. He has authored and coauthored more than 60 refereed journal and conference papers, and has been awarded five Chinese patents. His current research interests include the design of high power vertical-cavity surface-emitting lasers, III-V related material MOCVD growth, and diode laser applications.

Lijun Wang received the M.S. degree from the College of Electrical Science, Jilin University, Changchun, China, in 1973.

He was a Research Fellow with Jilin University until 1986. He joined the Changchun Institute of Optics, Fine Mechanics and Physics, Chinese Academy of Sciences, Changchun, China. From 1988 to 1989, he was with Swiss Postal Telegraph and Telephone Agency, Bern, Switzerland. From 1993 to 1995, he was a Senior Visiting Scholar with Northwestern University, Chicago, IL, USA. From 1995, he was a Leading Professor with the Changchun Institute of Optics. He has more than 30 years of experience in the research of the semiconductor laser theory, technology, and applications. He received the National Science and Technology Progress Award, National Technological Invention Award, and numerous other significant awards. He hosted and participated in 15 national and ministerial important projects, authorized 23 Chinese patents, published more than 300 papers, and three academic books. He was selected as the Member of Chinese Academy of Sciences in 2013. His current research interests include high power semiconductor lasers, vertical-cavity surface-emitting lasers, fiber-coupled diode lasers, and laser material processing.